Solution structure of IseA, an inhibitor protein of DL-endopeptidases from *Bacillus subtilis*, reveals a novel fold with a characteristic inhibitory loop*

Ryoichi Arai[‡§1], Sadaharu Fukui[‡], Naoya Kobayashi[‡], and Junichi Sekiguchi[‡2]

From the [‡]Division of Applied Biology, Faculty of Textile Science and Technology, and [§]International Young Researchers Empowerment Center, Shinshu University, Ueda, Nagano 386-8567, Japan

To whom correspondence should be addressed: Ryoichi Arai and Junichi Sekiguchi, Division of Applied Biology, Faculty of Textile Science and Technology, Shinshu University, Ueda, Nagano 386-8567, Japan, Tel & Fax: +81-268-21-5881 (R.A.), +81-268-21-5344 (J.S.); Email: rarai@shinshu-u.ac.jp (R.A.), jsekigu@shinshu-u.ac.jp (J.S.)

Key words: autolysin; DL-endopeptidase; inhibitor protein; new fold; NlpC/P60 family

Background: IseA from *Bacillus subtilis* is an inhibitor protein against DL-endopeptidases including synthetic lethal autolysins.
Results: We solved the solution structure of IseA using NMR. Titration with LytF DL-endopeptidase indicated interaction sites around the loop region.
Conclusion: The IseA structure revealed a novel "hacksaw"-like fold with a characteristic inhibitory loop.
Significance: The results suggest a new inhibition mechanism of IseA with a unique loop.

SUMMARY

In *Bacillus subtilis*, LytE, LytF, CwlS and CwlO are vegetative autolysins, DL-endopeptidases in the NlpC/P60 family, and play essential roles in cell growth and separation. IseA (YoeB) is a proteinaceous inhibitor against the DL-endopeptidases, peptidoglycan hydrolases. Overexpression of IseA caused significantly long-chained cell morphology, because IseA inhibits the cell-separation DL-endopeptidases post-translationally. Here we report the first three-dimensional structure of IseA, determined by NMR spectroscopy. The structure comprises a single domain consisting of three α-helices, one 3_{10}-helix and eight β-strands, which is a novel fold like a "hacksaw." Noteworthy is a dynamic loop between β4 and 3_{10}-helix, which resembles a "blade." The electrostatic potential distribution shows that most of the surface is positively charged, but the region around the loop is negatively charged. In contrast, the LytF active-site cleft is expected to be positively charged. NMR chemical shift perturbation of IseA interacting with LytF indicated that potential interaction sites are located around the loop. Furthermore, the IseA mutants D100K/D102K and G99P/G101P at the loop showed dramatic loss of inhibition activity against LytF, compared with wild-type IseA, indicating that the β4-3_{10} loop plays an important role in inhibition. Moreover, we built a complex structure model of IseA-LytF by docking simulation, suggesting that the β4-3_{10} loop of IseA gets stuck deep in the cleft of LytF and the active site is occluded. These results suggest a novel inhibition mechanism of the "hacksaw"-like structure, which is different from known inhibitor proteins, through interactions around the characteristic loop regions with the active-site cleft of enzymes.

The cell envelope of the Gram-positive bacterium, *Bacillus subtilis*, is composed of a single cytoplasmic membrane covered by a thick cell wall. The thick cell wall behaves as an exoskeleton, protecting the bacterium from many stresses. However, degradation of the cell wall is necessary for cell growth (1,2). In *B. subtilis*, proteins in the cell wall include not only synthetic enzymes of peptidoglycan but also autolytic enzymes of peptidoglycan, which are involved in cell wall turnover, cell growth, and cell separation (2,3). From the autolytic enzymes of *B. subtilis*, we have studied especially DL-endopeptidases, which hydrolyze the linkage of D-γ-glutamyl-*meso*-diaminopimelic acid in peptidoglycan. *B. subtilis* has four major

vegetative DL-endopeptidases, LytE, LytF, CwlS and CwlO (4-7), which are members of the NlpC/P60 protein domain family (Pfam entry, PF00877), a family of cell-wall cysteine peptidases (8). LytE, LytF and CwlS are cell separation autolysins (4-6), and the *lytE cwlO* genotype showed synthetic lethality (1,2). These enzymes have similar domain structures consisting of putative cell wall-binding domains, which are known as LysM repeats in LytE, LytF and CwlS, or an uncharacterized domain in CwlO, in the N-termini, and the catalytic domains of DL-endopeptidase in the C-termini (30-70% amino-acid identities). In addition, another DL-endopeptidase, PgdS from *B. subtilis*, is a poly-γ-glutamic acid degradase, which also belongs to the NlpC/P60 family (9).

Salzberg and Helmann reported that the cell surface protein, IseA (YoeB) from *B. subtilis*, was induced by cell-envelope targeting antibiotics (10). The *iseA* (*yoeB*) mutant exhibited an increased rate of autolysis in response to cell wall-targeting antibiotics or nutrient depletion, while a phenotypic difference between the deletion mutant and the wild type did not appear in the peptidoglycan structure or the levels of autolysins. Bisicchia *et al*. reported that *iseA* is one of the direct targets for negative regulation by YycF (WalR), a response regulator of the essential two-component system, YycFG (WalRK) (1,11).

In our previous study (12), we demonstrated that IseA is a proteinaceous inhibitor of the vegetative DL-endopeptidases, LytE, LytF, CwlS and CwlO, through direct interaction with their catalytic domains. Immunofluorescence microscopy with 3xFLAG-tag indicated that IseA localizes specifically at cell separation sites and cell poles on the vegetative cell surface in a similar manner of the DL-endopeptidases. Overexpression of IseA caused significantly long-chained cell morphology in the exponential growth phase, because IseA regulates the cell-separation DL-endopeptidases post-translationally.

Among proteinaceous inhibitors against cell wall lytic enzymes, Ivy family proteins, which inhibit vertebrate lysozymes and/or endogenous bacterial lytic transglycosylases, have been reported in Gram-negative bacteria (13-15). However, the amino-acid sequences of Ivy and IseA show no detectable homology, suggesting that the structure and inhibition mechanism of IseA should be different from Ivy. Many bacterial cell wall autolytic enzymes, including DL-endopeptidases and lytic transglycosylases, play essential roles in cell wall turnover, cell growth, and cell division (2,3,12,16). For instance, in *Listeria monocytogenes*, a food-borne pathogen, deletion of *iap* encoding p60, a cell wall lytic enzyme from the NlpC/P60 family, led to abnormal cell division and loss of actin-based motility, and the *iap* mutant was strongly attenuated in a mouse model after intravenous injection, demonstrating the importance of p60 during infection (17). Furthermore, the *lytE cwlO* genotype, whose protein products LytE and CwlO can be inhibited by IseA (2), led to synthetic lethality of *B. subtilis* (12). The bacterial cell wall autolytic enzymes should be tightly controlled within the producing cells because of their autolytic potential (16). These findings imply that understanding the inhibition and regulation mechanism of the cell wall lytic enzymes and their inhibitor proteins may contribute to development of antibacterial agents against new targets.

IseA homologs are present within several *Bacillus* and *Paenibacillus* species. For example, the *B. subtilis* IseA protein shares 77%, 76%, 65%, 50%, 47% and 32% amino-acid identity with the IseA homologs from *B. amyloliquefaciens*, *B. atrophaeus*, *B. licheniformis*, *B. pumilus*, *B. megaterium* and *Paenibacillus polymyxa*, respectively (Figure 1). However, IseA and its homologs do not show any significant similarity with protein domains of known three-dimensional (3D) structures. To understand the IseA inhibition mechanism, it is vital to solve its 3D structure. Here we report the first 3D structure of IseA from *B. subtilis*, determined by solution nuclear magnetic resonance (NMR)[3] spectroscopy. The structure shows a novel fold with a characteristic loop, and we suggest an inhibition mechanism of IseA against DL-endopeptidases.

EXPERIMENTAL PROCEDURES

Protein expression and purification – The DNA fragment encoding IseA (the original amino acid sequence from Lys24 to Ile181) was amplified from pQEYoeB (12) by PCR. The amplified DNA fragment was subcloned into the expression vector pCR2.1 (Life Technologies,

Carlsbad, CA) as a fusion with an N-terminal histidine affinity tag and a Tobacco etch virus (TEV) protease cleavage site. The uniformly $^{13}C/^{15}N$-labeled fusion protein was synthesized by a cell-free protein expression system (18-21). The cell-free reaction solution was first adsorbed to a HisTrap column (GE Healthcare, Little Chalfont, UK), which was washed with buffer A (20 mM Tris-HCl buffer, pH 8.0, containing 300 mM NaCl and 20 mM imidazole) and eluted with buffer B (20 mM Tris-HCl buffer, pH 8.0, containing 300 mM NaCl and 500 mM imidazole). To remove the histidine tag, the eluted protein was incubated at 297 K for 16 h with the TEV protease (22), producing a protein consisting of IseA residues K2-I159 (corresponding to the original residue numbers K24-I181 of *B. subtilis* IseA) with the first G1 of a cloning-artifact residue. After desalting with buffer A, the sample was applied to a HisTrap column. The flow-through fraction was fractionated on a HiTrap SP column by a concentration gradient of 20 mM Tris-HCl buffer (pH 8.0) containing 300 mM NaCl and 1 M NaCl, and the fractions containing IseA were collected. For NMR measurements, the purified protein was concentrated to 1.12 mM in 20 mM d-Tris buffer (pH 7.0), $^1H_2O/^2H_2O$ (9:1), containing 300 mM NaCl and 0.02% NaN_3.

NMR spectroscopy and resonance assignments – All NMR data were collected on Bruker AVANCE 600, 700 and 800 MHz spectrometers equipped with a triple-resonance CryoProbe at 298 K, at RIKEN NMR Facility (Tsurumi, Yokohama, Japan). Backbone and side-chain assignments were obtained by standard triple resonance experiments (23,24). 2D [^{1}H,^{15}N]-HSQC, and 3D HNCO, HN(CA)CO, HNCA, HN(CO)CA, HNCACB and CBCA(CO)NH spectra were used for the ^{1}H, ^{15}N and ^{13}C assignments of the protein backbone. Side-chain ^{1}H and ^{13}C assignments were obtained using 2D [^{1}H,^{13}C]-HSQC, and 3D HBHA(CO)NH, C(CCO)NH, HC(C)H-TOCSY, (H)CCH-TOCSY and HC(C)H-COSY spectra. All the assignments were checked for consistency with 3D ^{15}N- and ^{13}C-edited HSQC-NOESY spectra. 3D NOESY spectra were recorded with mixing times of 80 ms.

The NMR data were processed with the NMRPipe program (25). The programs KUJIRA (26) and NMRView (27,28) were used for visualization of the NMR spectra and for chemical shift assignments.

Structure calculations – Peak lists for the NOESY spectra were generated by interactive peak picking, and peak intensities were determined by the automatic integration function of NMRView (27,28). The 3D structure was determined by the combined automated NOESY cross-peak assignment and structure calculation with torsion angle dynamics implemented in the CYANA program (29). Restraints for the backbone torsion angles ϕ and ψ were determined by a chemical shift database analysis with the TALOS program (30). The structure calculations were started from 100 extended conformers, and the 20 conformers with the lowest final CYANA target function values were selected. The 20 structures from the CYANA calculation were subjected to restrained energy-refinement with the AMBER program (31). PROCHECK_NMR (32) was used to validate the final structures. Structure figures were prepared with the MOLMOL program (33) and PyMOL (DeLano Scientific).

Measurements of dynamic parameters and residual dipolar coupling (RDC) – The measurements of the nitrogen relaxation times, T_1 and T_2, and the proton-nitrogen heteronuclear NOEs were performed on a spectrometer using the ^{15}N,^{13}C-labeled IseA at a concentration of 1.12 mM. Relaxation delays of 10, 70, 150, 250, 370, 530, 760 and 1150 ms were recorded for the measurement of ^{15}N T_1, and relaxation delays of 14.4, 28.8, 43.2, 57.6, 72.0, 100.8, 144.0 and 187.2 ms were recorded for the measurement of ^{15}N T_2, using standard two-dimensional methods (34). The proton-nitrogen heteronuclear NOE values were calculated as the ratio between the cross-peak intensities with and without ^{1}H saturation during relaxation delays.

RDC was obtained using [^{1}H,^{15}N]-IPAP HSQC spectra under the isotropic and anisotropic (polyacrylamide gel) conditions (35).

NMR titration experiments – The 6×His-tagged LytF catalytic domain (LytF) was expressed and purified with a HisTrap HP column (GE healthcare), as described previously (5). LytF was further purified by cation exchange chromatography (20 mM MES buffer, pH 6.5, with a linear gradient of NaCl from 0.1 to 2 M) with a Poros HS/M column (Perseptive Biosystems) and gel filtration chromatography (20 mM MES buffer, pH 6.5, containing 150 mM

NaCl) with a Superdex 75 10/300 GL column (GE healthcare). For the amide chemical shift titration experiments, the catalytic domain of purified LytF was prepared in 20 mM d-Tris buffer (pH 7.0), $^{1}H_2O/^{2}H_2O$ (9:1), containing 300 mM NaCl and 0.02% NaN_3. 2D [^{1}H,^{15}N]-HSQC spectra were recorded on Bruker AVANCE 600 and 700 MHz spectrometers with LytF domain concentrations relative to the IseA concentration (0.06 mM) to the ratio of IseA:LytF = 1:0, 1:0.5, 1:1 and 1:2.

Cell wall hydrolase assay – Expression vectors of the IseA mutants were made from pQEYoeB (12), using megaprimer PCR. The IseA mutants with 6×His-tag were expressed in *Escherichia coli* and purified using TALON metal affinity resin (Clontech, Mountain View, CA), and cell wall hydrolase assays were performed as described previously (12). Briefly, the reaction mixture comprised *B. subtilis* cell wall (final OD_{540} = 0.3) in 20 mM MES-NaOH buffer (pH 6.5) containing 100 mM KCl, and was pre-incubated at 37°C. The protein mixtures containing the catalytic domain of LytF (1 nmol) and each IseA variant (2 nmol) (mutants, D100N/D102N, D100K/D102K, G99P/G101P, or wild-type) were pre-incubated in the buffer at 37°C for 5 min. Then each protein mixture was added to the reaction mixture (final volume 2 mL) in a cuvette with a stirrer. The OD_{540} of the reaction mixture was measured at 37°C with a spectrophotometer (V-560; JASCO, Tokyo, Japan).

Homology Modeling and Docking Simulation – The structure models of the catalytic domains were predicted by homology modeling using the SWISS-MODEL program (http://swissmodel.expasy.org/) (36-38). The template structure was the structure of lipoprotein Spr from *E. coli* (residues 36-164; PDB ID, 2K1G) (39). Moreover, a structure model of IseA and the LytF catalytic domain complex was predicted by docking simulation using the docking web server GRAMM-X (http://vakser.bioinformatics.ku.edu/resources/gramm/grammx) (40,41). The protein docking software GRAMM-X and its web interface extended the original GRAMM Fast Fourier Transformation methodology (42-44) by employing smoothed potentials, refinement stage, and knowledge-based scoring (40,41).

RESULTS

Structure determination – First, we tried to crystallize the IseA protein to solve the 3D structure by X-ray crystallography. However, we obtained only thin microcrystals with almost no X-ray diffraction. Thus, we performed NMR spectroscopy experiments to determine the structure of IseA.

We measured a complete set of standard 2D and 3D NMR spectra (23,24). The 2D [^{1}H,^{15}N]-HSQC spectrum of the IseA showed dispersed, sharp NH signals with similar intensities, which are characteristic of a folded protein (Figure 2A). One disulfide bond between C40 and C56 was confirmed by their proton nuclear Overhauser effect (NOE) peaks and the chemical shifts of their Cβ atoms, which were 44.59 ppm and 47.33 ppm, respectively (45).

More than 20 NOE distance restraints per residue, including 1320 long-range distance restraints, were used in the final structure calculations with the CYANA program (29). The final structures were energy-refined with the AMBER program (31). The final 20 energy-minimized conformers that represent the solution structure of IseA were well defined (Figure 2B) and showed excellent agreement with the statistical data (Table 1). The precision of the structure was characterized by root-mean-square deviation (RMSD) values to the mean coordinates of 0.40 Å for the backbone and 0.66 Å for all heavy atoms, excluding the unstructured regions of residues G1–D7 at the N-termini (Figure 2B). In the ordered regions, which include Q10–M28 (α1), T44–Y47 (β1), L50–Y54 (β2), K62–L69 (α2), K75–K83 (α3), T88–S90 (β3), K93–P97 (β4), W107–K109 [η1(3_{10}-helix)], T111–K118 (β5), T121–V128 (β6), A137–K145 (β7) and W150–V152 (β8), the RMSD values to the mean coordinates were 0.25 Å for the backbone and 0.53 Å for all heavy atoms, respectively. The quality of the structure is also reflected by the fact that 89.8% of the (ϕ,ψ) backbone torsion angle pairs were found in the favored regions and 9.9% were within the additionally allowed regions of the Ramachandran plot, according to the PROCHECK_NMR program (32).

Moreover, to confirm the reliability of the IseA structure, we performed RDC analysis with polyacrylamide gel (Figure S1 in Supplemental

Data). This analysis also supported the high accuracy of the IseA structure determined by NMR.

Overall structure of IseA – The solution structure of the IseA protein comprises a single domain consisting of three α-helices (α1, α2 and α3), two anti-parallel β-sheets (β1, β2, β4 and β3; β5, β6, β7 and β8), and one 3_{10}-helix (η1) (Figures 1 and 2C). One disulfide bond, C40-C56, forms a bridge between the two loops, α1-β1 and β2-α2. The three α-helices constitute a backbone structure in the central region. Each of the two anti-parallel β-sheets is located on the two polar ends of the α-helices. A particularly noteworthy region is the loop (G99-N103) between β4 and 3_{10}-helix (η1).

The structural homology search results against the IseA structure by the DALI server (46) revealed several structures whose Z-scores were above 5 (Figure 3). However, unlike the separated two β-sheets of IseA, these structures have one continuous β-sheet, suggesting that the IseA structure has a novel fold.

The electrostatic potential distribution (Figure 4A) and the highly conserved residues (Figure 4B) on the solvent-accessible surface of the IseA structure clearly show the negatively-charged and conserved region around the β4-3_{10} loop (G99-N103), suggesting that the region is probably important for the function. Interestingly, the loop and the rest of the structure make a through-hole within the IseA structure (Figure 4). The uncommon framework structure of IseA looks like a "hacksaw," in which the three α-helices constitute a backbone frame, the two β-sheets make a side frame, and the acidic loop resembles a "blade."

Dynamic properties of the IseA – To determine the dynamic properties of the IseA structure, the ^{15}N T_1 and T_2 relaxation times and the steady-state ^{1}H-^{15}N NOEs were measured at 298 K (Figure 5). The average NOE values for the α- and 3_{10}-helices, β-sheets, and C-terminal regions were above 0.8. These values are in agreement with the result that these regions are tightly packed to form a rigid body in solution. The NOE values for the N-terminal extension before α1 decreased gradually when approaching the chain terminus, indicating that the N-terminal region is intrinsically disordered in solution. The lower NOE values, shorter T_1, and longer T_2, for the two loop regions, α1-β1 (K36-G43) and β4-3_{10} (G99-N103), compared with the above-mentioned rigid core, indicate that the two loop regions are flexible and dynamic. Incidentally, these flexible and dynamic N-terminal and loop regions may be the cause for the difficulty to crystallize IseA.

Titration of IseA with the catalytic domain of LytF – To investigate the interaction site of IseA with the catalytic domain of DL-endopeptidases, we performed 2D [^{1}H,^{15}N]-HSQC titration experiments with the addition of the LytF catalytic domain (LytF). Figure 6A shows the 2D [^{1}H,^{15}N]-HSQC spectra of samples whose molar ratios of IseA:LytF were 1:0 (black), 1:0.5 (red), 1:1 (green) and 1:2 (blue). The addition of LytF to IseA induced chemical shift changes in the HSQC spectra of IseA. The spectra, in the cases of the 1:1 and 1:2 ratios, were very similar, suggesting that IseA mostly forms the 1:1 stoichiometric complex with LytF under the 1:1 and 1:2 ratio conditions in the NMR experiments. The close-up view of the dotted-line rectangle (in Figure 6A) is shown in Figure 6B. The left panel of Figure 6B shows that the addition of the LytF to IseA (IseA:LytF = 1:0.5) induced a reduction in peak intensity of the original IseA (e.g., A, B, C, and A157) and an emergence of new peaks (e.g., A', B', C', and D'), probably derived from the IseA-LytF complex in the 2D [^{1}H,^{15}N]-HSQC spectrum. In the case of IseA:LytF = 1:2 (Figure 6B, right panel), the original peaks of IseA (A, B, C, and A157) disappeared, and the intensity of the new peaks (A', B', C', and D') increased. These new peaks of IseA:LytF = 1:0.5 and 1:2 completely overlapped, suggesting that the interaction between IseA and LytF is in slow exchange on the NMR timescale. Furthermore, after the addition of LytF, there were several peaks such as A157, which we could not trace in the 2D [^{1}H,^{15}N]-HSQC spectrum because their chemical shift changes were too big. These untraceable peaks, including H23, F24, W25, M28, S29, G30, H31, I98, G99, G101, D102, L105, W107, T130, D132, G133, N153, F155, A157 and I159 (Figure 6A), suggest that these residues are involved in the interaction between IseA and LytF, directly or indirectly. These residues are located at the β4-3_{10} loop, the β6-β7 loop, the latter half of α1, and the C-terminus of the IseA structure (Figure 7), suggesting that the surface regions interacting

with LytF are distributed around the β4-3_{10} loop.

Cell wall hydrolase assay – Based on these results, we speculated that the acidic and dynamic β4-3_{10} loop of IseA is important for the inhibition of DL-endopeptidases. To test this speculation, we performed site-directed mutagenesis at the β4-3_{10} loop and inhibition analysis of cell wall hydrolase assay. We made three IseA mutants: D100N/D102N and D100K/D102K changed the negative charge on the β4-3_{10} loop to a neutral and positive charge, respectively, and G99P/G101P restricted the flexibility and structure of the β4-3_{10} loop. Figure 8 shows the inhibition activities of the IseA mutants against LytF cell wall lysis. The IseA mutants D100K/D102K and G99P/G101P showed dramatic loss of inhibition activity against LytF, compared with wild-type IseA, suggesting that the β4-3_{10} loop plays an important role in the inhibition of the enzyme, while the D100N/D102N mutant showed almost the same inhibition activity as wild-type IseA.

DISCUSSION

Structural and Surface Properties of Catalytic Domains of DL-Endopeptidases, Predicted by Homology Modeling – To speculate about the interaction mechanism between IseA and the catalytic domains of the target DL-endopeptidases, model structures of the catalytic domains were predicted by homology modeling using the SWISS-MODEL program (36-38). The template structure was the structure of lipoprotein Spr from *E. coli* (residues 36-164; PDB ID, 2K1G) (39), which is a member of the NlpC/P60 protein domain family (Pfam entry, PF00877) (8) and shares 38%, 34%, 33%, 30% and 36% identity with the catalytic domains of LytF, LytE, CwlS, CwlO and PgdS, respectively (Figure 9A). Global model quality estimation of these homology-modeling structures by QMEAN (47) showed reasonable QMEAN scores (LytF, 0.62; LytE, 0.59; CwlS, 0.59; PgdS, 0.61) and QMEAN Z-scores (LytF, -1.8; LytE, -2.1; CwlS, -2.1; PgdS, -2.0) except for CwlO (QMEAN score, 0.47; QMEAN Z-score, -3.5), suggesting that we can discuss global structure and surface properties of some DL-endopeptidases using the homology-modeling structures (Figure 9B).

Structural analyses of Spr (39), AvPCP and NpPCP endopeptidases from cyanobacteria (48), and YkfC from *B. cereus* (BcYkfC) (49), from the NlpC/P60 family, showed a characteristic Cys-His-His catalytic triad in the active sites of these cysteine peptidases. In the deduced active sites of LytF, LytE, CwlS, CwlO and PgdS (shown as red arrowheads in Figures 9A, B), the first and second residues, Cys and His, are strictly conserved (Figure 9A), but the third residue is His in LytE and CwlS, Asn in LytF and CwlO, and Gln in PgdS. Indeed, we demonstrated that the conserved cysteine residues of LytE and CwlO are essential for their enzymatic activity (2). Generally, in cysteine proteases/peptidases, the two residues of the active site, Cys and His, catalyze the hydrolysis reaction (50). Thus, the deduced catalytic triads of LytF, LytE, CwlS, CwlO and PgdS probably work as the catalytic residues.

Figure 9D shows the electrostatic potential distribution on the solvent-accessible surface of the homology-modeling structures of the DL-endopeptidases. The dashed-line ellipses indicate their active-site cleft regions. These figures suggest that the surface regions around the active-site cleft of LytF, LytE, CwlS and CwlO are significantly positively charged. However, the surface region around the active-site cleft of PgdS is neutral or negatively charged, relative to the others.

Inhibition mechanism of IseA against the catalytic domains of DL-endopeptidases – As shown in Figure 9D, the surface regions around the enzymatic active sites of the DL-endopeptidases, except PgdS, are positively charged. The negatively-charged region of IseA around the β4-3_{10} loop (Figure 9C), which widely overlaps with the potential LytF-interacting regions according to the NMR titration experiment (Figure 7B), is complementary to the positively-charged regions around the active sites of the DL-endopeptidases, except PgdS. This is consistent with the preliminary experimental result that IseA did not inhibit the enzymatic activity of PgdS (Sekiguchi et al., unpublished data), while IseA inhibited the enzymatic activity of LytF, LytE, CwlS and CwlO (12). Furthermore, in the surface configurations, the narrow and stretch structure of the IseA β4-3_{10} loop, looking like a "blade" of a "hacksaw," is a complementary shape to the narrow and long cleft of the enzymatic active site of the DL-endopeptidases (Figure 9D). Therefore, we propose the hypothesis

that the acidic and dynamic IseA β4-3_{10} loop occludes specifically the active-site cleft of DL-endopeptidases, and also the acidic surface regions around the loop widely interact with the basic surface around the active site of the enzyme, as suggested by the NMR titration experiment (Figure 7), i.e., IseA inhibits the enzymatic activity by not only the β4-3_{10} loop occupying the active site but also IseA widely blocking the regions around the active site and the substrate biding site.

To partially test this hypothesis, we performed site-directed mutagenesis (D100N/D102N, D100K/D102K, and G99P/G101P) of IseA and inhibition analysis against LytF. Figure 8 demonstrates that the IseA mutants D100K/D102K and G99P/G101P showed dramatic loss of inhibition activity compared with wild-type IseA, indicating that the β4-3_{10} loop plays an important role in the inhibition mechanism. In addition, the D100N/D102N mutant showed almost the same inhibition activity as the wild-type IseA. The inhibition activity of the D100N/D102N mutant seemed to be contradictory to the abovementioned hypothesis about charge complementation. However, we speculate that D100 and/or D102 of IseA may be recognized by LytF not through basic residues but polar residues, which are compatible with the D100N/D102N mutation. In the crystal structure of BcYkfC complexed with the reaction product, L-Ala-γ-D-Glu, the α-carboxyl of D-Glu was recognized by hydrogen-bond interactions with the side chains of S239 and S257 (49). Because the S239 residue next to the catalytic cysteine is strictly conserved among the homologs (shown by a blue arrowhead in Figure 9A), S401 of LytF, corresponding to S239 of BcYkfC, may also recognize the α-carboxyl of D-Glu of the peptidoglycan substrate. In addition, we speculate that the β-carboxyl of L-Asp (D100 or D102) of IseA may mimic the α-carboxyl of D-Glu of the substrate, recognized by a hydrogen bond with S401 of LytF, and a side-chain amide of Asn (D100N or D102N) of the IseA mutant (D100N/D102N) may be compatibly recognized by a hydrogen bond with S401 of LytF.

In contrast, the structures and inhibition mechanisms of several proteinaceous inhibitors such as cystatin and chagasin against cysteine proteases/peptidases have been reported (51,52). The structure of cystatin from chicken egg white consists of one α-helix and one anti-parallel β-sheet, and the structure of chagasin from the parasite *Trypanosoma cruzi* consists of two anti-parallel β-sheets known as an immunoglobulin-like β-sandwich fold. Although the overall structures of cystatin and chagasin are different, they bind to the same class of cysteine proteases via remarkably similar tripartite interactions using short loops and the N-terminus (51). However, the structure of IseA is clearly distinct from the structures of cystatin and chagasin, and our interaction and mutagenesis analyses suggest that the inhibition mechanism of IseA is different from that of cystatin and chagasin.

Moreover, the structures of cathepsin L cysteine proteases with their propeptides from human and *Toxoplasma gondii* have been reported (53,54). The amino acid sequences of the propeptides bound to the active-site cleft are MNGFQ (residues 75p-79p) from human and YLGFK (residues 177p-181p) from *T. gondii*. The structures shows that the binding regions of the propeptides to the active-site cleft of cathepsin L form strained conformation, and the binding mode contains hydrogen bonds and hydrophobic interactions. The β4-3_{10} loop sequence of IseA is GDGDN (residues 99-103), which plays an important role in the inhibition mechanism. The IseA β4-3_{10} loop also has glycine residues, and it is a flexible and dynamic loop without secondary structure. However, the IseA β4-3_{10} loop has no hydrophobic side chains in contrast to the binding regions of the cathepsin L propeptides, suggesting that the binding mechanism of IseA is different from that of the propeptides of cathepsin L.

In addition, the structure of *E. coli* Ivyc, a lysozyme inhibitor protein in the Ivy family, complexed with hen egg white lysozyme (HEWL) has been reported (13). Through the complex formation, the lysozyme active site becomes occluded by a loop protruding from the Ivyc molecule. The loop is relatively rigid because it consists of the conserved amino acid sequence, CKPHDC (residues 57-62), in which there is a disulfide bridge between the two Cys residues and a salt bridge between the Lys and Asp residues. Conversely, the IseA β4-3_{10} loop, which looks like

a "hacksaw blade," is a flexible and dynamic (Figures 2B and 5)., These contrasts suggest that the inhibition mechanism of IseA is also distinct from that of Ivyc.

Finally, to visualize the proposed novel inhibition mechanism, we present a model of the complex structure of IseA and the LytF catalytic domain, predicted by the GRAMM-X docking simulation program, which employs a smoothed Lennard-Jones potential on a fine grid during the global search FFT stage, followed by the refinement optimization in continuous coordinates and rescoring with several knowledge-based potential terms (40,41). The complex structure model of IseA-LytF shows that the $\beta 4\text{-}3_{10}$ loop of IseA gets stuck deep in the cleft of LytF and the active site is physically occupied (Figure 10). Figure 10B shows that most of the potential interacting residues (shown as magenta stick models), indicated by the NMR titration experiment, are proximately nestled around the wide surface of LytF, suggesting that the complex structure model is plausible.

In conclusion, the first 3D structure of IseA determined by NMR reveals a novel fold with a characteristic inhibitory loop, suggesting a novel inhibition mechanism against DL-endopeptidases. The present study provides the mechanistic insights into the *B. subtilis* cell growth and separation events controlled post-translationally by the molecular interactions between IseA and DL-endopeptidases. To understand the recognition mechanism in atomic level, further studies are necessary.

REFERENCES

1. Bisicchia, P., Noone, D., Lioliou, E., Howell, A., Quigley, S., Jensen, T., Jarmer, H., and Devine, K. M. (2007) *Mol. Microbiol.* **65**, 180-200
2. Hashimoto, M., Ooiwa, S., and Sekiguchi, J. (2012) *J. Bacteriol.* **194**, 796-803
3. Smith, T. J., Blackman, S. A., and Foster, S. J. (2000) *Microbiology* **146**, 249-262
4. Ishikawa, S., Hara, Y., Ohnishi, R., and Sekiguchi, J. (1998) *J. Bacteriol.* **180**, 2549-2555
5. Ohnishi, R., Ishikawa, S., and Sekiguchi, J. (1999) *J. Bacteriol.* **181**, 3178-3184
6. Fukushima, T., Afkham, A., Kurosawa, S., Tanabe, T., Yamamoto, H., and Sekiguchi, J. (2006) *J. Bacteriol.* **188**, 5541-5550
7. Yamaguchi, H., Furuhata, K., Fukushima, T., Yamamoto, H., and Sekiguchi, J. (2004) *J. Biosci. Bioeng.* **98**, 174-181
8. Anantharaman, V., and Aravind, L. (2003) *Genome Biol.* **4**, R11
9. Suzuki, T., and Tahara, Y. (2003) *J. Bacteriol.* **185**, 2379-2382
10. Salzberg, L. I., and Helmann, J. D. (2007) *J. Bacteriol.* **189**, 4671-4680
11. Bisicchia, P., Lioliou, E., Noone, D., Salzberg, L. I., Botella, E., Hubner, S., and Devine, K. M. (2010) *Mol. Microbiol.* **75**, 972-989
12. Yamamoto, H., Hashimoto, M., Higashitsuji, Y., Harada, H., Hariyama, N., Takahashi, L., Iwashita, T., Ooiwa, S., and Sekiguchi, J. (2008) *Mol. Microbiol.* **70**, 168-182
13. Abergel, C., Monchois, V., Byrne, D., Chenivesse, S., Lembo, F., Lazzaroni, J. C., and Claverie, J. M. (2007) *Proc. Natl. Acad. Sci. USA* **104**, 6394-6399
14. Monchois, V., Abergel, C., Sturgis, J., Jeudy, S., and Claverie, J. M. (2001) *J. Biol. Chem.* **276**, 18437-18441
15. Clarke, C. A., Scheurwater, E. M., and Clarke, A. J. (2010) *J. Biol. Chem.* **285**, 14843-14847
16. Pfeffer, J. M., Moynihan, P. J., Clarke, C. A., and Clarke, A. J. (2012) Control of lytic transglycosylase activity within bacterial cell walls. in *Bacterial Glycomics* (Reid, C. W., Twine, S. M., and Reid, A. N. eds.), Caister Academic Press, Norfolk, UK. pp 55-68
17. Pilgrim, S., Kolb-Maurer, A., Gentschev, I., Goebel, W., and Kuhn, M. (2003) *Infect. Immun.* **71**, 3473-3484
18. Kigawa, T., Yabuki, T., Yoshida, Y., Tsutsui, M., Ito, Y., Shibata, T., and Yokoyama, S. (1999) *FEBS Lett.* **442**, 15-19
19. Kigawa, T., Yabuki, T., Matsuda, N., Matsuda, T., Nakajima, R., Tanaka, A., and Yokoyama, S. (2004) *J. Struct. Funct. Genomics* **5**, 63-68
20. Matsuda, T., Kigawa, T., Koshiba, S., Inoue, M., Aoki, M., Yamasaki, K., Seki, M., Shinozaki, K., and Yokoyama, S. (2006) *J. Struct. Funct. Genomics* **7**, 93-100

21. Matsuda, T., Koshiba, S., Tochio, N., Seki, E., Iwasaki, N., Yabuki, T., Inoue, M., Yokoyama, S., and Kigawa, T. (2007) *J. Biomol. NMR* **37**, 225-229
22. Kapust, R. B., Tozser, J., Fox, J. D., Anderson, D. E., Cherry, S., Copeland, T. D., and Waugh, D. S. (2001) *Protein Eng.* **14**, 993-1000
23. Clore, G. M., and Gronenborn, A. M. (1994) *Methods Enzymol.* **239**, 349-363
24. Bax, A. (1994) *Curr. Opin. Struct. Biol.* **4**, 738-744
25. Delaglio, F., Grzesiek, S., Vuister, G. W., Zhu, G., Pfeifer, J., and Bax, A. (1995) *J. Biomol. NMR* **6**, 277-293
26. Kobayashi, N., Iwahara, J., Koshiba, S., Tomizawa, T., Tochio, N., Guntert, P., Kigawa, T., and Yokoyama, S. (2007) *J. Biomol. NMR* **39**, 31-52
27. Johnson, B. A., and Blevins, R. A. (1994) *J. Biomol. NMR* **4**, 603-614
28. Johnson, B. A. (2004) *Methods Mol. Biol.* **278**, 313-352
29. Güntert, P. (2004) *Methods Mol. Biol.* **278**, 353-378
30. Cornilescu, G., Delaglio, F., and Bax, A. (1999) *J. Biomol. NMR* **13**, 289-302
31. Case, D. A., Cheatham, T. E., 3rd, Darden, T., Gohlke, H., Luo, R., Merz, K. M., Jr., Onufriev, A., Simmerling, C., Wang, B., and Woods, R. J. (2005) *J. Comput. Chem.* **26**, 1668-1688
32. Laskowski, R. A., Rullmannn, J. A., MacArthur, M. W., Kaptein, R., and Thornton, J. M. (1996) *J. Biomol. NMR* **8**, 477-486
33. Koradi, R., Billeter, M., and Wuthrich, K. (1996) *J Mol Graph* **14**, 51-55
34. Farrow, N. A., Muhandiram, R., Singer, A. U., Pascal, S. M., Kay, C. M., Gish, G., Shoelson, S. E., Pawson, T., Forman-Kay, J. D., and Kay, L. E. (1994) *Biochemistry* **33**, 5984-6003
35. Ottiger, M., Delaglio, F., and Bax, A. (1998) *J. Magn. Reson.* **131**, 373-378
36. Bordoli, L., Kiefer, F., Arnold, K., Benkert, P., Battey, J., and Schwede, T. (2009) *Nat. Protoc.* **4**, 1-13
37. Kiefer, F., Arnold, K., Kunzli, M., Bordoli, L., and Schwede, T. (2009) *Nucleic Acids Res.* **37**, D387-392
38. Arnold, K., Bordoli, L., Kopp, J., and Schwede, T. (2006) *Bioinformatics* **22**, 195-201
39. Aramini, J. M., Rossi, P., Huang, Y. J., Zhao, L., Jiang, M., Maglaqui, M., Xiao, R., Locke, J., Nair, R., Rost, B., Acton, T. B., Inouye, M., and Montelione, G. T. (2008) *Biochemistry* **47**, 9715-9717
40. Tovchigrechko, A., and Vakser, I. A. (2005) *Proteins* **60**, 296-301
41. Tovchigrechko, A., and Vakser, I. A. (2006) *Nucleic Acids Res.* **34**, W310-314
42. Vakser, I. A., and Aflalo, C. (1994) *Proteins* **20**, 320-329
43. Katchalski-Katzir, E., Shariv, I., Eisenstein, M., Friesem, A. A., Aflalo, C., and Vakser, I. A. (1992) *Proc. Natl. Acad. Sci. USA* **89**, 2195-2199
44. Vakser, I. A. (1995) *Protein Eng.* **8**, 371-377
45. Sharma, D., and Rajarathnam, K. (2000) *J. Biomol. NMR* **18**, 165-171
46. Holm, L., and Rosenstrom, P. (2010) *Nucleic Acids Res.* **38**, W545-549
47. Benkert, P., Biasini, M., and Schwede, T. (2011) *Bioinformatics* **27**, 343-350
48. Xu, Q., Sudek, S., McMullan, D., Miller, M. D., Geierstanger, B., Jones, D. H., Krishna, S. S., Spraggon, G., Bursalay, B., Abdubek, P., Acosta, C., Ambing, E., Astakhova, T., Axelrod, H. L., Carlton, D., Caruthers, J., Chiu, H. J., Clayton, T., Deller, M. C., Duan, L., Elias, Y., Elsliger, M. A., Feuerhelm, J., Grzechnik, S. K., Hale, J., Han, G. W., Haugen, J., Jaroszewski, L., Jin, K. K., Klock, H. E., Knuth, M. W., Kozbial, P., Kumar, A., Marciano, D., Morse, A. T., Nigoghossian, E., Okach, L., Oommachen, S., Paulsen, J., Reyes, R., Rife, C. L., Trout, C. V., van den Bedem, H., Weekes, D., White, A., Wolf, G., Zubieta, C., Hodgson, K. O., Wooley, J., Deacon, A. M., Godzik, A., Lesley, S. A., and Wilson, I. A. (2009) *Structure* **17**, 303-313
49. Xu, Q., Abdubek, P., Astakhova, T., Axelrod, H. L., Bakolitsa, C., Cai, X., Carlton, D., Chen, C., Chiu, H. J., Chiu, M., Clayton, T., Das, D., Deller, M. C., Duan, L., Ellrott, K., Farr, C. L., Feuerhelm, J., Grant, J. C., Grzechnik, A., Han, G. W., Jaroszewski, L., Jin, K. K., Klock, H. E., Knuth, M. W., Kozbial, P., Krishna, S. S., Kumar, A., Lam, W. W., Marciano, D., Miller, M. D., Morse, A. T., Nigoghossian, E., Nopakun, A., Okach, L., Puckett, C., Reyes, R., Tien, H. J., Trame, C. B., van den Bedem, H., Weekes, D., Wooten, T., Yeh, A., Hodgson, K. O., Wooley, J., Elsliger, M. A., Deacon, A. M., Godzik, A., Lesley, S. A., and Wilson, I. A. (2010) *Acta Crystallogr. F Struct. Biol. Cryst. Comm.* **66**, 1354-1364
50. Drenth, J., Jansonius, J. N., Koekoek, R., and Wolthers, B. G. (1971) *Adv. Protein Chem.* **25**, 79-115
51. Wang, S. X., Pandey, K. C., Scharfstein, J., Whisstock, J., Huang, R. K., Jacobelli, J., Fletterick, R. J., Rosenthal, P. J., Abrahamson, M., Brinen, L. S., Rossi, A., Sali, A., and McKerrow, J. H. (2007) *Structure* **15**, 535-543
52. Wang, S. X., Pandey, K. C., Somoza, J. R., Sijwali, P. S., Kortemme, T., Brinen, L. S., Fletterick, R. J., Rosenthal, P. J., and McKerrow, J. H. (2006) *Proc. Natl. Acad. Sci. USA* **103**, 11503-11508

53. Coulombe, R., Grochulski, P., Sivaraman, J., Menard, R., Mort, J. S., and Cygler, M. (1996) *EMBO J.* **15**, 5492-5503
54. Larson, E. T., Parussini, F., Huynh, M. H., Giebel, J. D., Kelley, A. M., Zhang, L., Bogyo, M., Merritt, E. A., and Carruthers, V. B. (2009) *J. Biol. Chem.* **284**, 26839-26850
55. Petersen, T. N., Brunak, S., von Heijne, G., and Nielsen, H. (2011) *Nat. Methods* **8**, 785-786
56. Gouet, P., Courcelle, E., Stuart, D. I., and Metoz, F. (1999) *Bioinformatics* **15**, 305-308
57. Larkin, M. A., Blackshields, G., Brown, N. P., Chenna, R., McGettigan, P. A., McWilliam, H., Valentin, F., Wallace, I. M., Wilm, A., Lopez, R., Thompson, J. D., Gibson, T. J., and Higgins, D. G. (2007) *Bioinformatics* **23**, 2947-2948
58. Kabsch, W., and Sander, C. (1983) *Biopolymers* **22**, 2577-2637
59. Hoelz, A., Nairn, A. C., and Kuriyan, J. (2003) *Mol. Cell* **11**, 1241-1251
60. Cushman, I., Bowman, B. R., Sowa, M. E., Lichtarge, O., Quiocho, F. A., and Moore, M. S. (2004) *J. Mol. Biol.* **344**, 303-310
61. Motoyama, T., Nakasako, M., and Yamaguchi, I. (2002) *Acta Crystallogr. D Biol. Crystallogr.* **58**, 148-150

Acknowledgments – We are grateful to Yasuko Tomo, Takushi Harada, Takeshi Nagira, Manami Sato, Hua Li, Naoya Tochio, Seizo Koshiba, Satoru Watanabe and Takanori Kigawa at RIKEN SSBC for protein expression/purification, NMR experiments and NMR data analyses, which were performed at NMR Facility, RIKEN Yokohama Institute. We thank Chikashi Kitaura for sample preparation and preliminary crystallization, and Masayuki Hashimoto and Takaaki Sato for valuable discussion. We also thank the staff of the Structural Biology Beamlines at the Photon Factory, KEK, for the preliminary X-ray diffraction experiment, which was performed under the approval of the Photon Factory program advisory committee (Proposal No. 2008G511 and 2008G512).

FOOTNOTES

*This work was supported by Grants-in-Aid for Scientific Research (KAKENHI) (B) (19380047) and (A) (22248008) to J.S., and Grants-in-Aid for Scientific Research on Innovative Areas (22113508 and 24113707) and for Young Scientists (B) (24780097), and Program for Dissemination of Tenure-Track System to R.A., funded by Japan Society for the Promotion of Science (JSPS) and the Ministry of Education, Culture, Sports, Science and Technology (MEXT) of Japan.

[S]This article contains supplemental Fig. S1.

The atomic coordinates (code 2RSX) have been deposited in the Protein Data Bank, Research Collaboratory for Structural Bioinformatics, Rutgers University, New Brunswick, NJ (http://www.rcsb.org/).

[1]To whom correspondence may be addressed: Tel. & Fax: 81-268-21-5881; Email: rarai@shinshu-u.ac.jp.
[2]To whom correspondence may be addressed: Tel. & Fax: 81-268-21-5344; Email: jsekigu@shinshu-u.ac.jp.

[3]The abbreviations used are: COSY, Correlation Spectroscopy; HSQC, heteronuclear single quantum correlation; NMR, nuclear magnetic resonance; NOESY, nuclear Overhauser effect spectroscopy; NOE, nuclear Overhauser effect; RDC, residual dipolar coupling; RMSD, root-mean-square deviation; TEV, Tobacco etch virus; TOCSY, Total Correlation Spectroscopy.

FIGURE LEGENDS

FIGURE 1. Amino-acid sequence alignment of homologs of *Bacillus subtilis* IseA (YoeB).
B. subtilis IseA (YoeB) homologs are derived from *Bacillus amyloliquefaciens* FZB42, *Bacillus atrophaeus* 1942, *Bacillus licheniformis* ATCC 14580, *Bacillus pumilus* ATCC 7061, *Bacillus sp.* NRRL B-14911, *Bacillus megaterium* DSM 319, and *Paenibacillus polymyxa* SC2. Their deduced signal peptide sequences, predicted by SignalP 4.0 (55), are omitted. The alignment was generated by ESPript (56) with ClustalW2 (57). The secondary structures of the IseA structure determined by NMR are shown above (α, α-helix; β, β-strand; η, 3_{10}-helix; TT, β-turn) as analyzed by DSSP (58). Green symbols at the bottom indicate a disulfide bond. The amino-acid sequence of "*B. subtilis* (NMR)" is the *B. subtilis* IseA protein expression construct used for the NMR experiments in this study. The first residue G1 is a cloning artifact residue. The full-length sequence of the original IseA (YoeB) from *B. subtilis* (strain 168) consists of 181 amino-acid residues, including 23 residues of the signal peptide (M1- A23) predicted by SignalP. In this study, the original residue numbers K24-I181 of *B. subtilis* IseA were renumbered K2-I159 of the IseA expression construct for the NMR experiments.

FIGURE 2. Structural analysis of *B. subtilis* IseA using NMR spectroscopy.
(A) 2D [^{1}H,^{15}N]-HSQC spectrum of IseA. The spectrum was recorded at a ^{1}H frequency of 800 MHz (pH 7.0) at 298 K. Cross-peaks are labeled with the residue numbers. Side-chain resonances of asparagine and glutamine residues are indicated by horizontal lines.
(B) Backbone traces of the 20 energy-minimized conformers of the solution structure of IseA (stereoview).
(C) Ribbon representation of the IseA structure (stereoview). Color gradient (blue, green, yellow, red) from N-terminus to C-terminus. A disulfide bond between C40 and C56 is shown as stick models.

FIGURE 3. Structural homology search results of the IseA structure.
Representative structures of 3D structural homologs (Z-score > 5) searched by the DALI server (46). These structures are shown as a monomer.
(A) The solution structure of IseA from *B. subtilis*.
(B) Crystal structure of hypothetical protein YybH from *B. subtilis* (Northeast Structural Genomics Consortium, unpublished).
(C) Crystal structure of the association domain of Ca^{2+}/calmodulin-dependent kinase II from *Mus musculus* (59).
(D) Crystal structure of nuclear transport carrier NTF2 from *Rattus norvegicus* (60).
(E) Crystal structure of scytalone dehydratase from *Magnaporthe grisea* (61).

FIGURE 4. Surface presentation of the IseA structure.
(A) The electrostatic potential distribution on the solvent-accessible surface of the IseA structure. Blue and red surfaces represent positive and negative potentials, respectively. The potentials were calculated at ±3 kT/e using the PyMOL APBS Tools (Lerner, M., 2004).
(B) Residue conservation mapping on the surface of the IseA structure. Magenta and orange surfaces represent completely and highly conserved residues on the solvent-accessible surface of the IseA structure, respectively.

The views at both sides were made by ±90° vertical axis rotation. The arrowheads indicate the strictly conserved D100-G101 region at the β4-3_{10} loop.

FIGURE 5. NMR analysis of dynamic properties of IseA.
(A) ^{15}N T_1 relaxation time of IseA.
(B) ^{15}N T_2 relaxation time of IseA.
(C) The steady-state ^{1}H-^{15}N NOEs of IseA.

These data suggest that the N-terminal region and the two loop regions, α1-β1 (K36-G43) and β4-3_{10}

(G99-N103), are flexible and dynamic.

FIGURE 6. Titration of IseA with the catalytic domain of LytF.
(A) The 2D [^{1}H,^{15}N]-HSQC spectra of the samples whose molar ratios of IseA:LytF (catalytic domain) were 1:0 (black), 1:0.5 (red), 1:1 (green), and 1:2 (blue).
(B) The close-up view of 2D [^{1}H,^{15}N]-HSQC spectra in the dotted-line rectangle (in Figure 6A). The left panel shows the spectra after the addition of LytF to IseA at a ratio of 1:0.5 (IseA:LytF), and the right panel shows the spectra after the addition of LytF to IseA at a ratio of 1:2.

FIGURE 7. Mapping of the untraceable peak residues in the titration experiment on the IseA structure (stereoviews).
The residues of the untraceable peaks in the 2D [^{1}H,^{15}N]-HSQC spectra are shown as magenta stick models with labels. The (B) view was made by 90° vertical axis rotation of the (A) view.

FIGURE 8. Cell wall hydrolytic curves of DL-endopeptidases with the IseA Mutants.
The cell wall hydrolytic curves. LytF catalytic domain (LytF) only (gray line), LytF and wild-type IseA (black line), LytF and IseA mutants: D100N/D102N (green line), D100K/D102K (blue line), or G99P/G101P (red line).

FIGURE 9. Homology modeling of catalytic domains of DL-endopeptidases.
(A) Sequence alignment of catalytic domains of lipoprotein Spr from *E. coli*, DL-endopeptidases LytF, LytE, CwlS, CwlO and PgdS, from *B. subtilis*, AvPCP from *A. variabilis*, and BcYkfC from *B. cereus*. The deduced catalytic triad residues are shown as red arrowheads below the alignment. The secondary structures of the Spr structure (PDB ID, 2K1G) (39) are shown above (α, α-helix; β, β-strand; η, 3_{10}-helix; TT, β-turn) as analyzed by DSSP.
(B) The superimposition of the main-chain structure models of the catalytic domains of DL-endopeptidases, predicted by homology modeling using SWISS-MODEL. LytF (residues 370-488; green), LytE (residues 230-334; cyan), CwlS (residues 297-414; magenta), CwlO (residues 340-472; orange), PgdS (residues 64-286; yellow), and Spr (residues 36-164; gray; PDB 2K1G). The deduced catalytic triad residues are shown as stick models and indicated by red arrowheads.
(C) The electrostatic potential distribution on the solvent-accessible surface of the IseA structure. Blue and red surfaces represent positive and negative potentials, respectively. The potentials were calculated at ±3 kT/e using the PyMOL APBS Tools. The dashed-line ellipse indicates the β4-3_{10} loop region of IseA.
(D) The electrostatic potential distribution on the solvent-accessible surface of the homology structure models of the catalytic domains of DL-endopeptidases. Blue and red surfaces represent positive and negative potentials, respectively. The potentials were calculated at ±3 kT/e using the PyMOL APBS Tools. The dashed-line ellipses indicate their active-site cleft regions.

FIGURE 10. Structure model of the complex of IseA and the LytF catalytic domain.
(A) Ribbon representation of a complex structure model of IseA (red) and the LytF catalytic domain (cyan), predicted by GRAMM-X docking simulation (40,41) (stereoview). The deduced catalytic triad (C400, H449 and N461) of LytF is shown as stick models and indicated by arrowheads.
(B) The complex structure model is represented as the electrostatic potential surface of LytF, and ribbon representation of IseA with the potential interacting residues (shown as magenta stick models) suggested by the NMR titration experiment. The view of IseA is the same as in Figure 7A. Blue and red surfaces of LytF represent positive and negative potentials, respectively. The potentials were calculated at ±3 kT/e using the PyMOL APBS Tools.

Table 1. Summary of conformational restraints and statistics of the final 20 structures

NOE upper distance limits	
Total	3659
Intra residue (|i-j| = 0)	852
Sequential (|i-j| = 1)	836
Medium range (1< |i-j| < 5)	651
Long range (|i-j| >= 5)	1320
Torsion angle restraints	154
CYANA target function value 0.24	
Distance restraint violations	
Number > 0.1 Å	0
Maximum (Å)	-
Torsion angle restraint violations	
Number > 5°	0
Maximum (°)	-
Energies of AMBER calculation (kcal/mol)	
Mean AMBER energy	-4076.34
Ramachandran plot statistics[a]	
Residues in favored regions	89.8%
Residues in additionally allowed regions	9.9%
Residues in generously allowed regions	0.2%
Residues in disallowed regions	0.1%
RMS deviation to the averaged coordinates	
All regions[b]	
Backbone atoms (Å)	0.40
Heavy atoms (Å)	0.66
Ordered regions[c]	
Backbone atoms (Å)	0.25
Heavy atoms (Å)	0.53

[a] The region for the PROCHECK calculation includes L8–I159.
[b] "All regions" include L8–I159.
[c] "Ordered regions" include Q10–M28 (α1), T44–Y47 (β1), L50–Y54 (β2), K62–L69 (α2), K75–K83 (α3), T88–S90 (β3), K93–P97 (β4), W107–K109 (3_{10}), T111–K118 (β5), T121–V128 (β6), A137–K145 (β7), W150–V152 (β8).

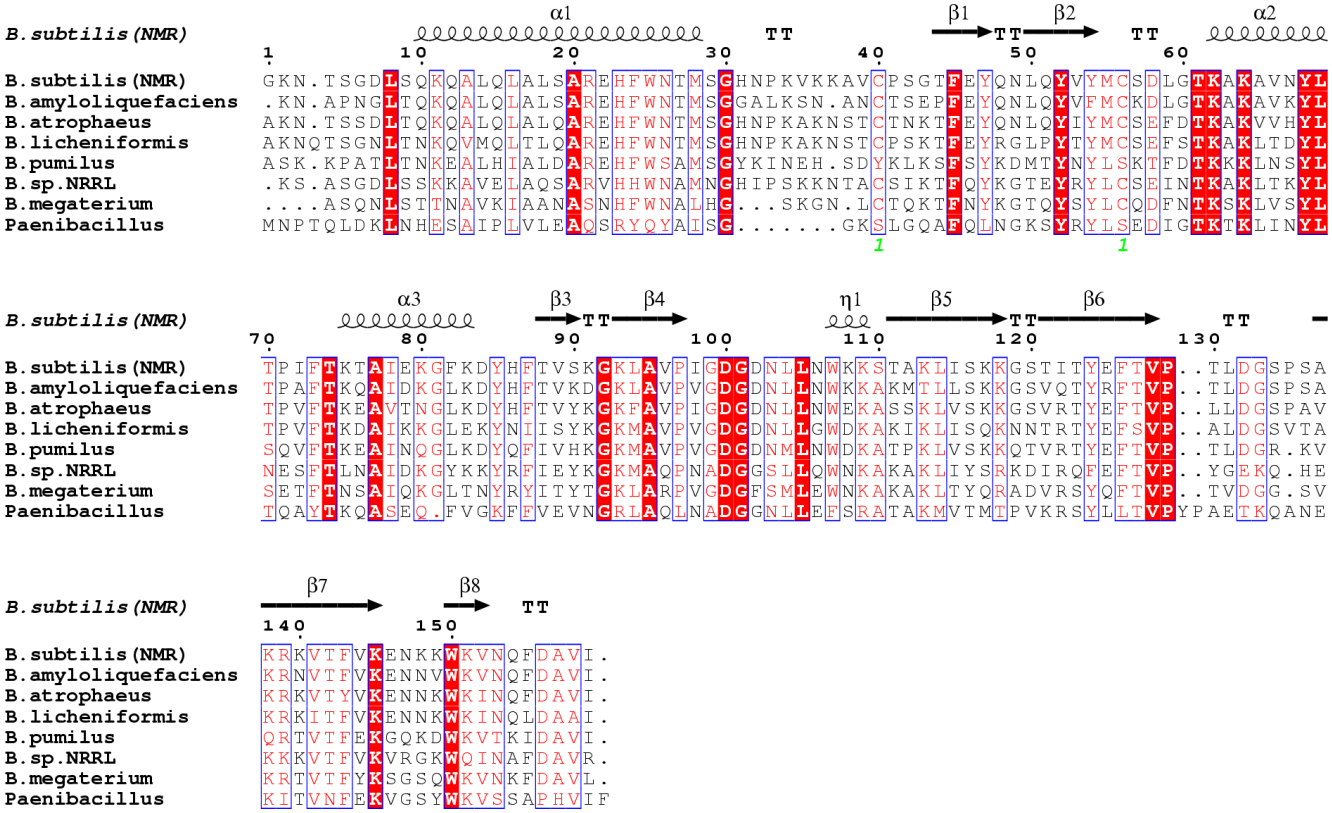

Fig. 1, R. Arai et al., NMR Structure of IseA

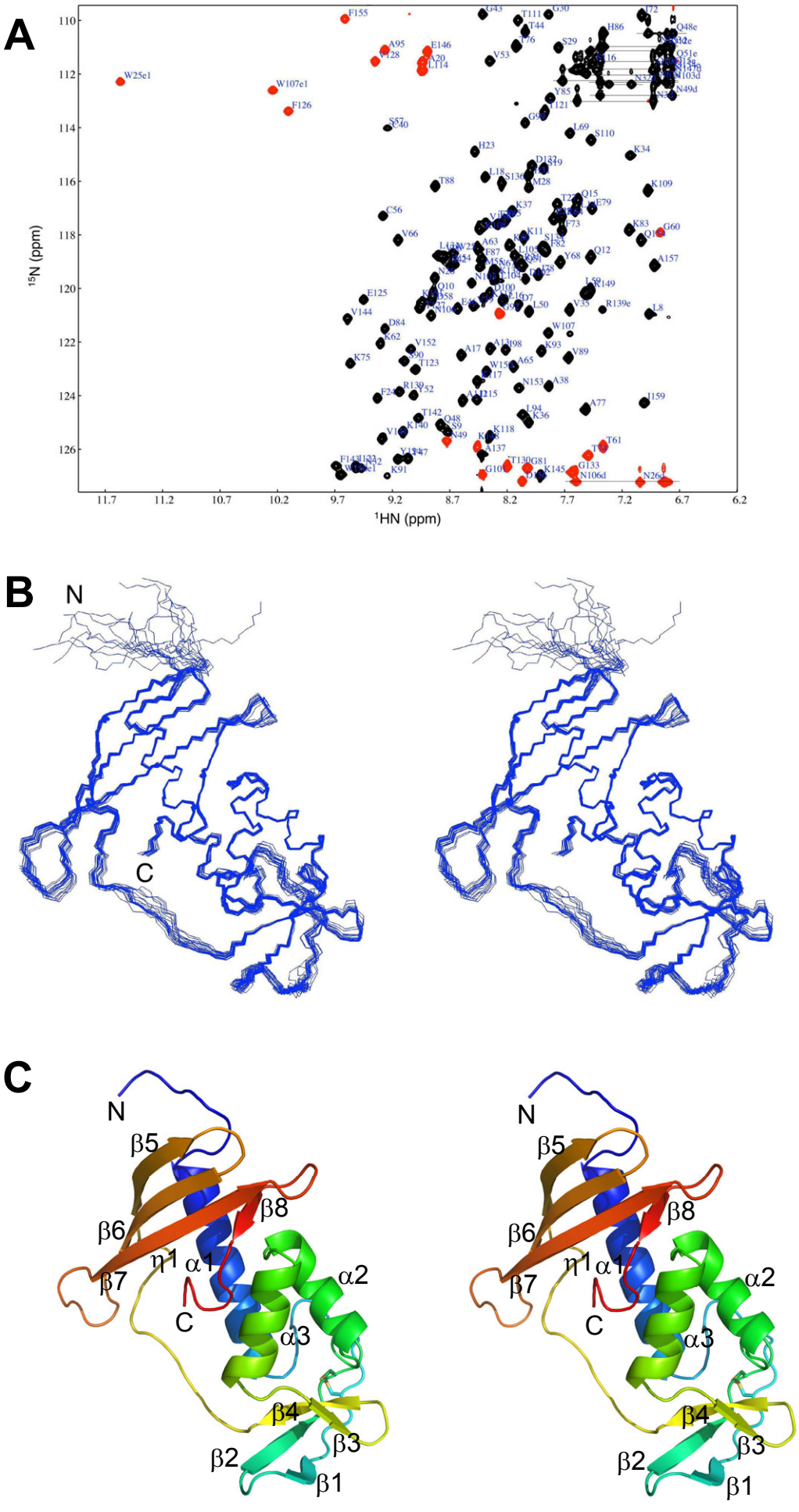

Fig. 2, R. Arai et al., NMR Structure of IseA

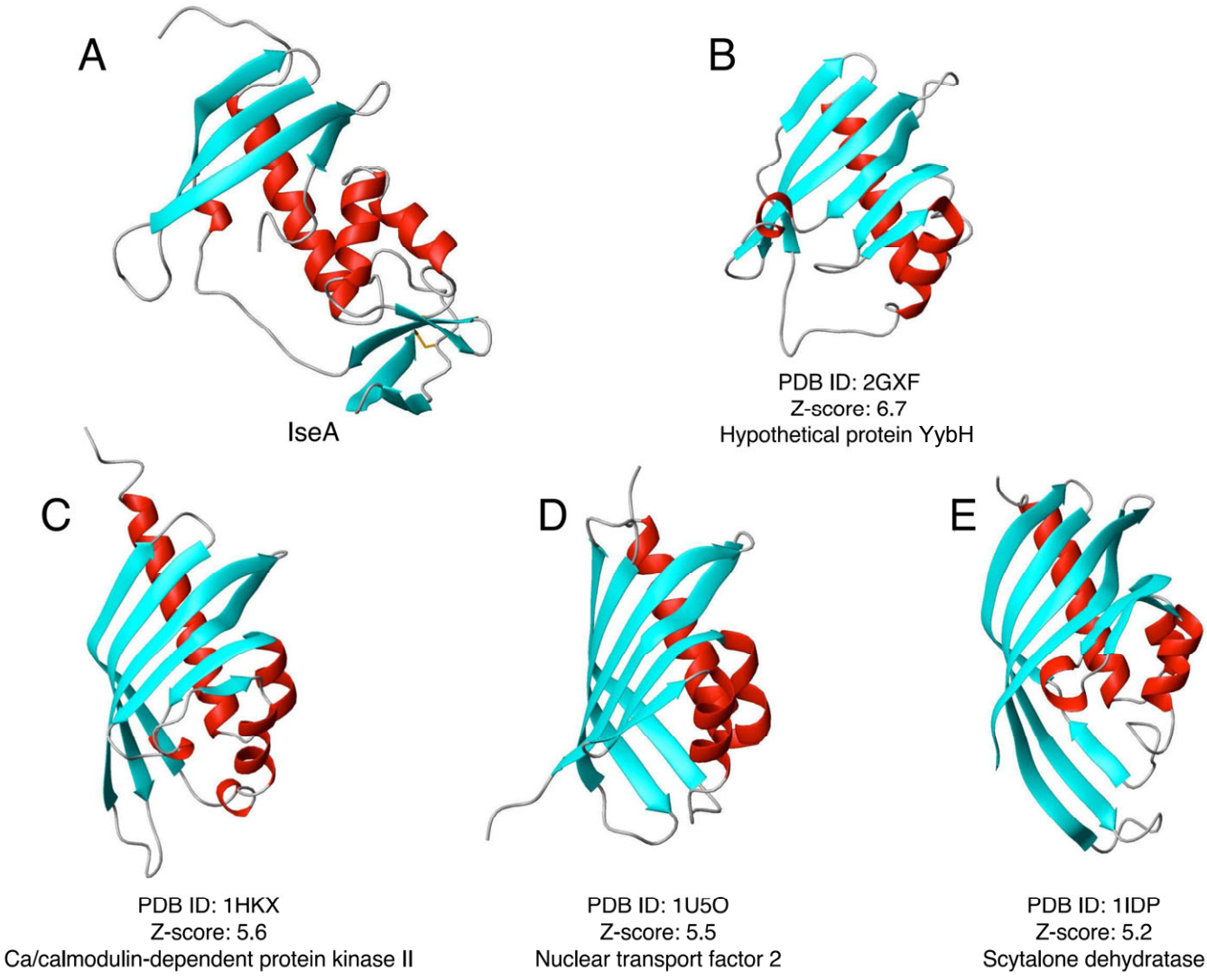

Fig. 3, R. Arai et al., NMR Structure of IseA

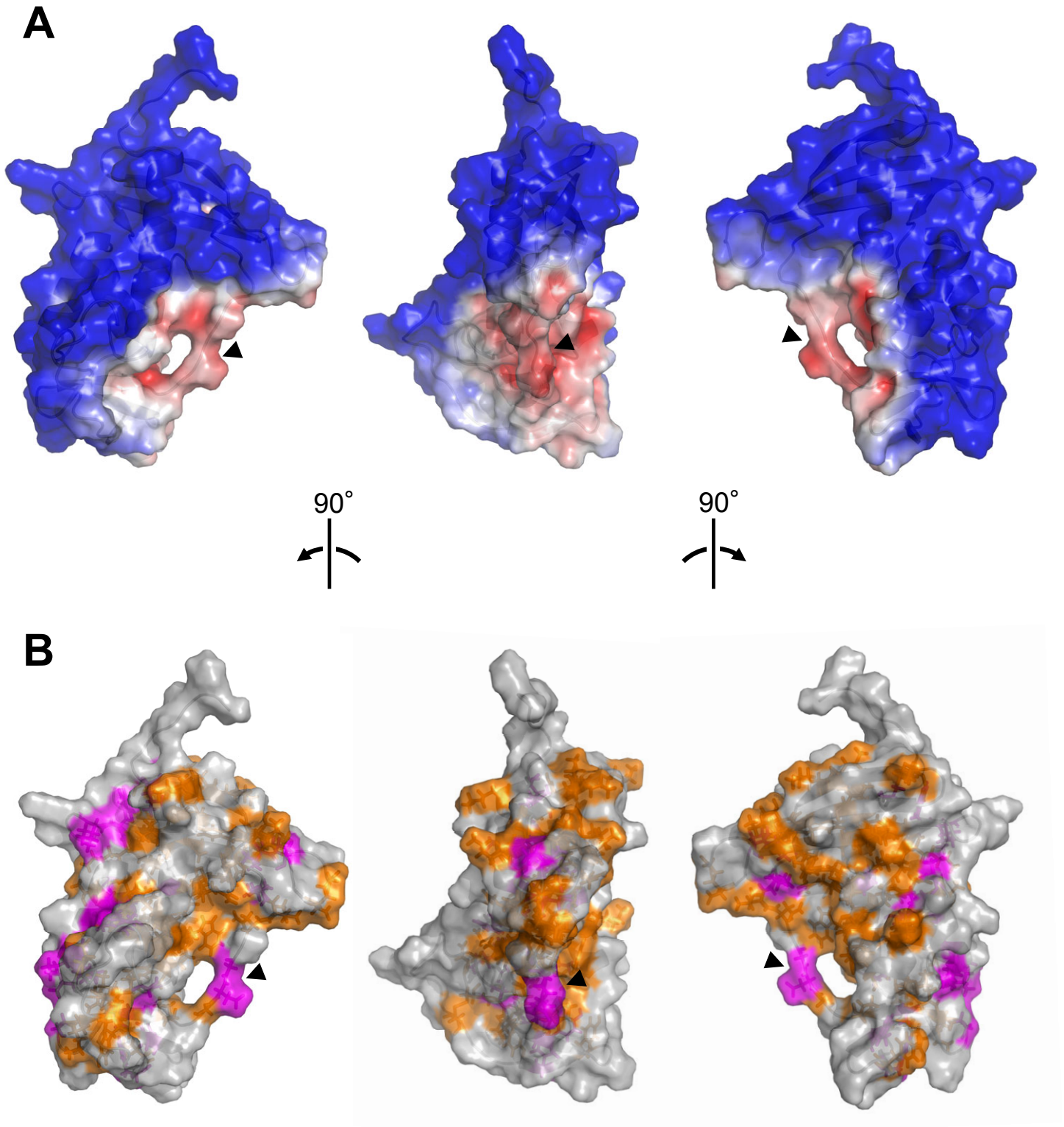

Fig. 4, R. Arai et al., NMR Structure of IseA

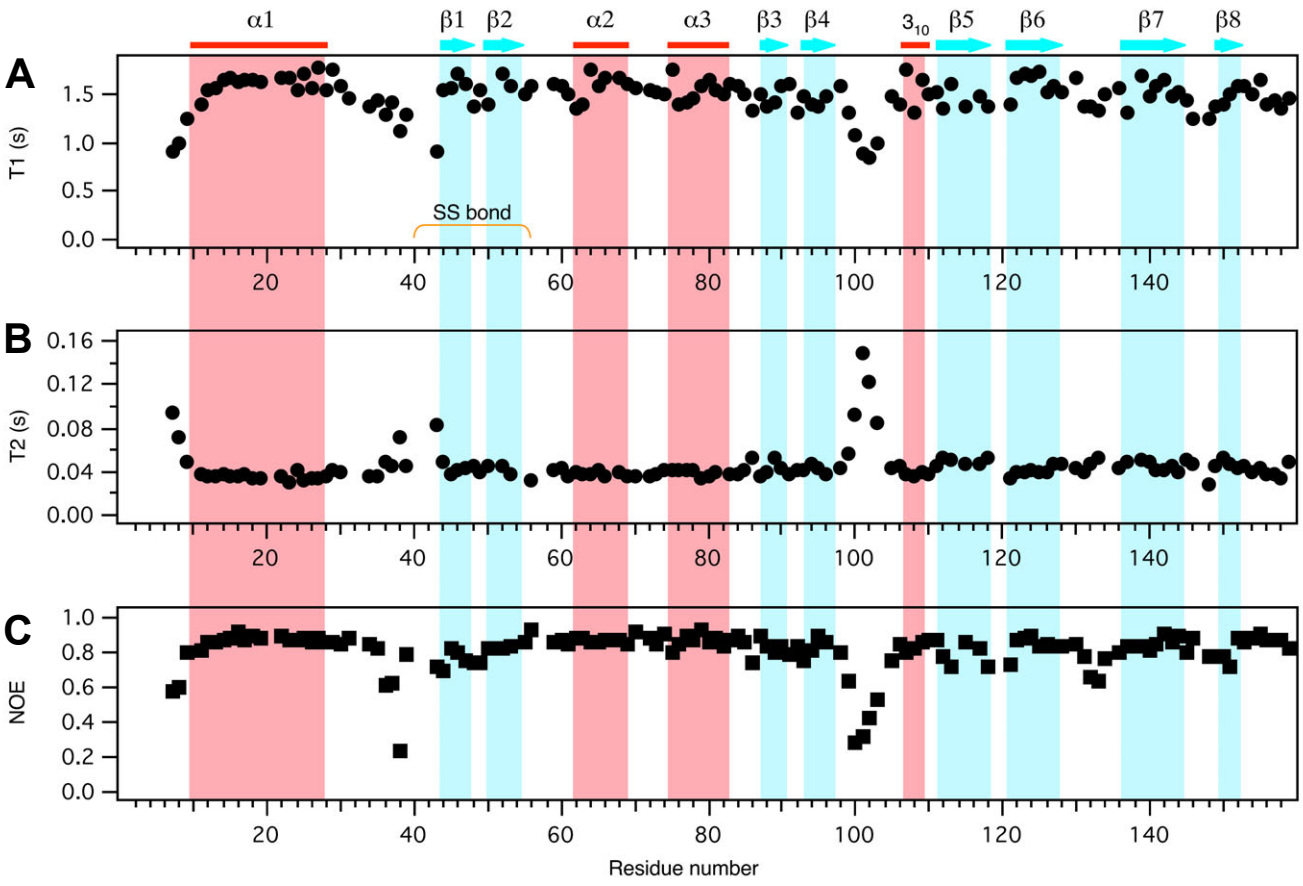

Fig. 5, R. Arai et al., NMR Structure of IseA

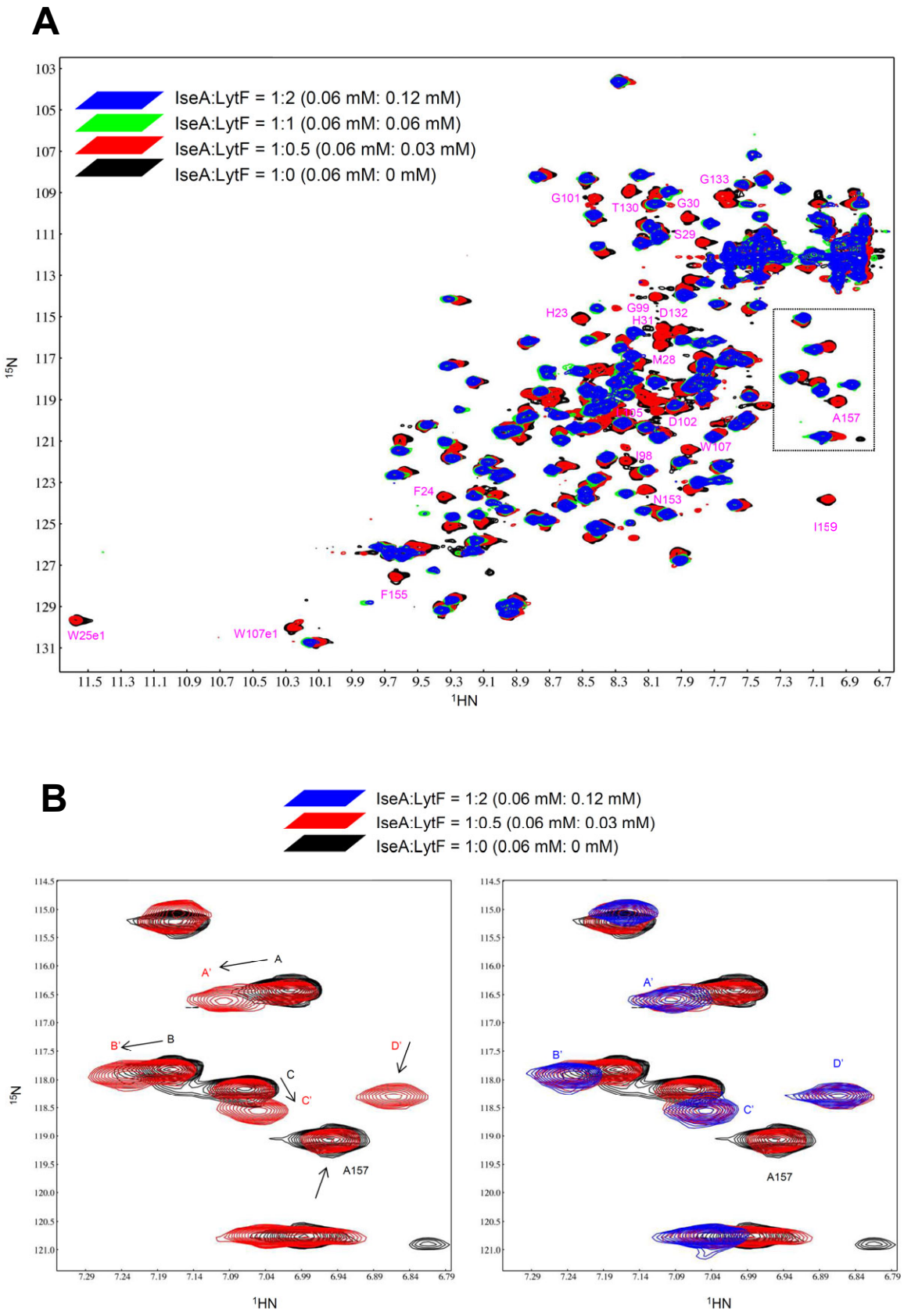

Fig. 6, R. Arai et al., NMR Structure of IseA

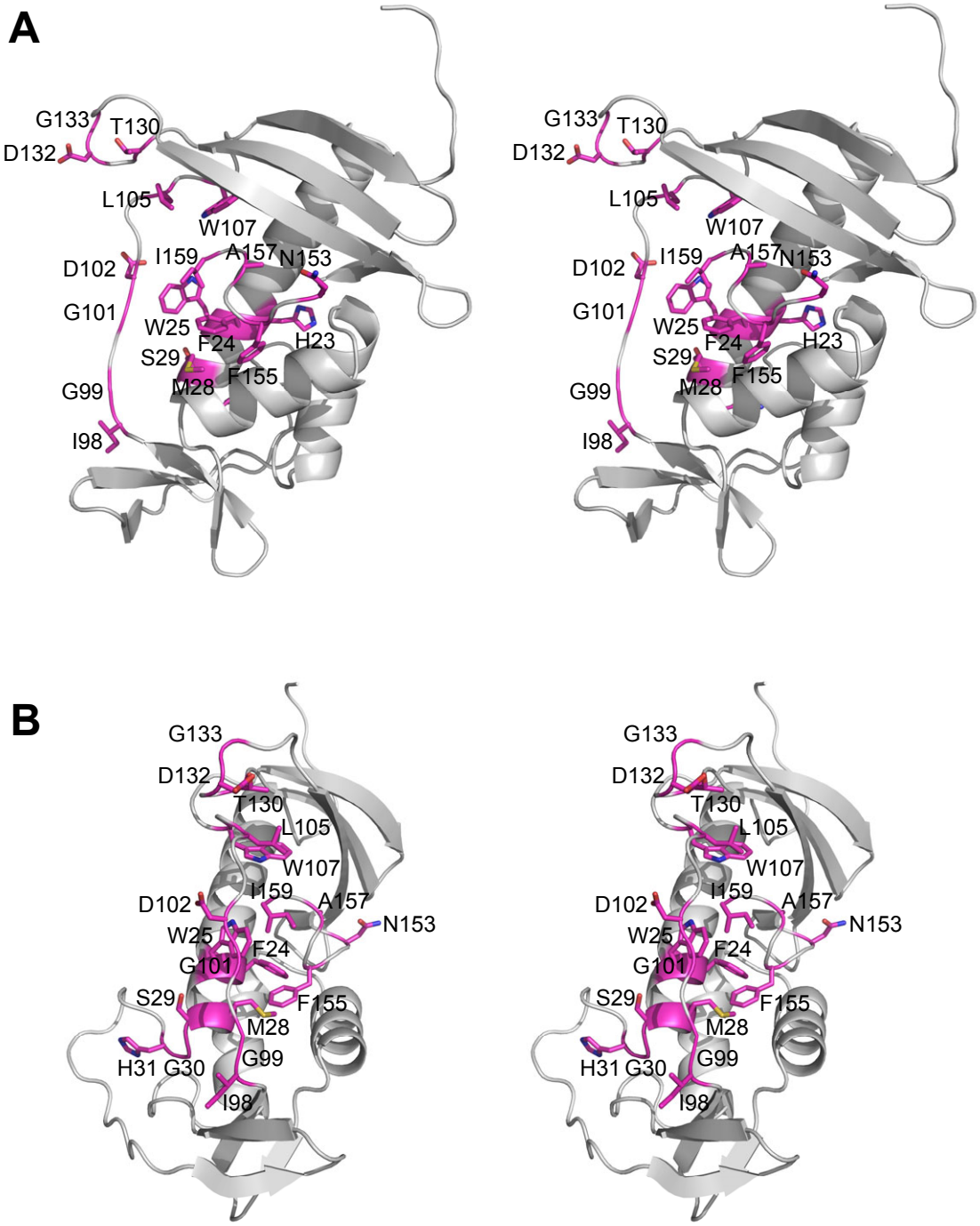

Fig. 7, R. Arai et al., NMR Structure of IseA

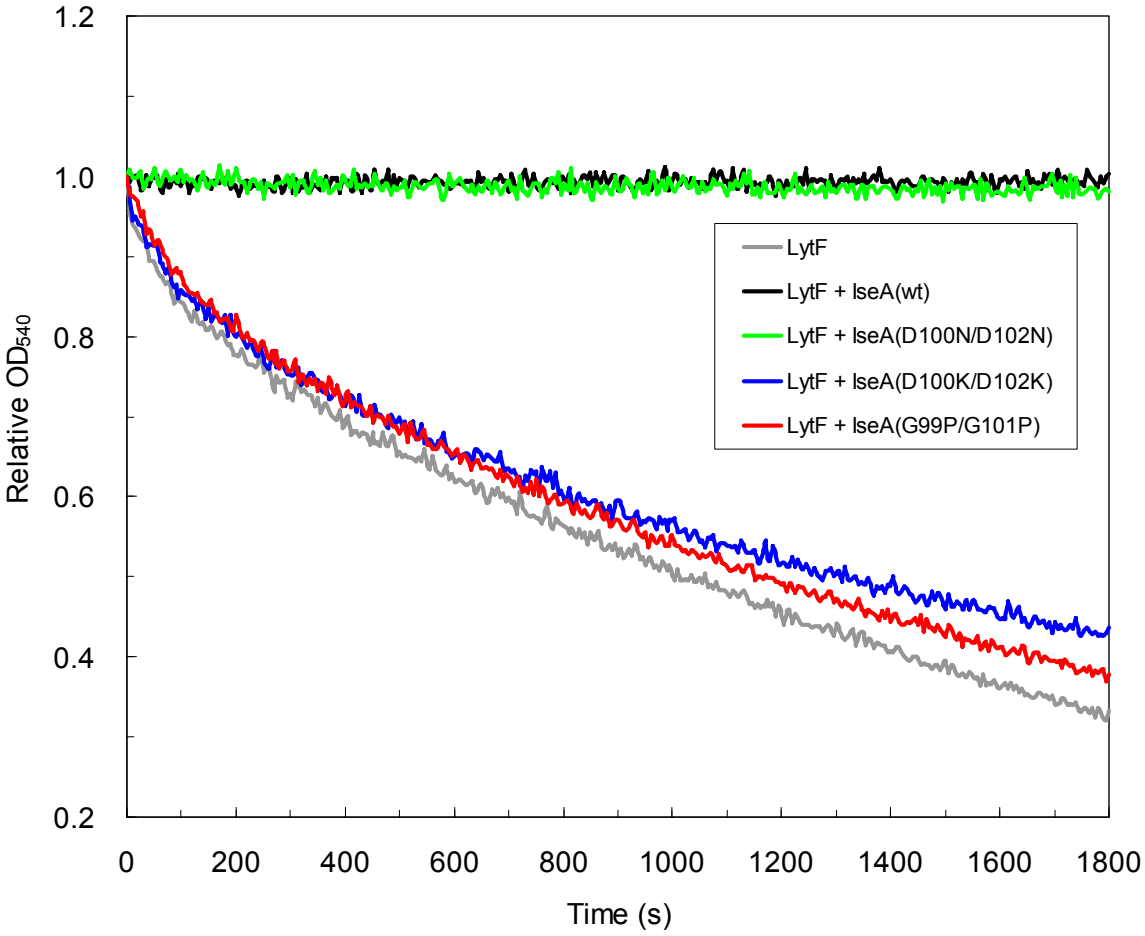

Fig. 8, R. Arai et al., NMR Structure of lseA

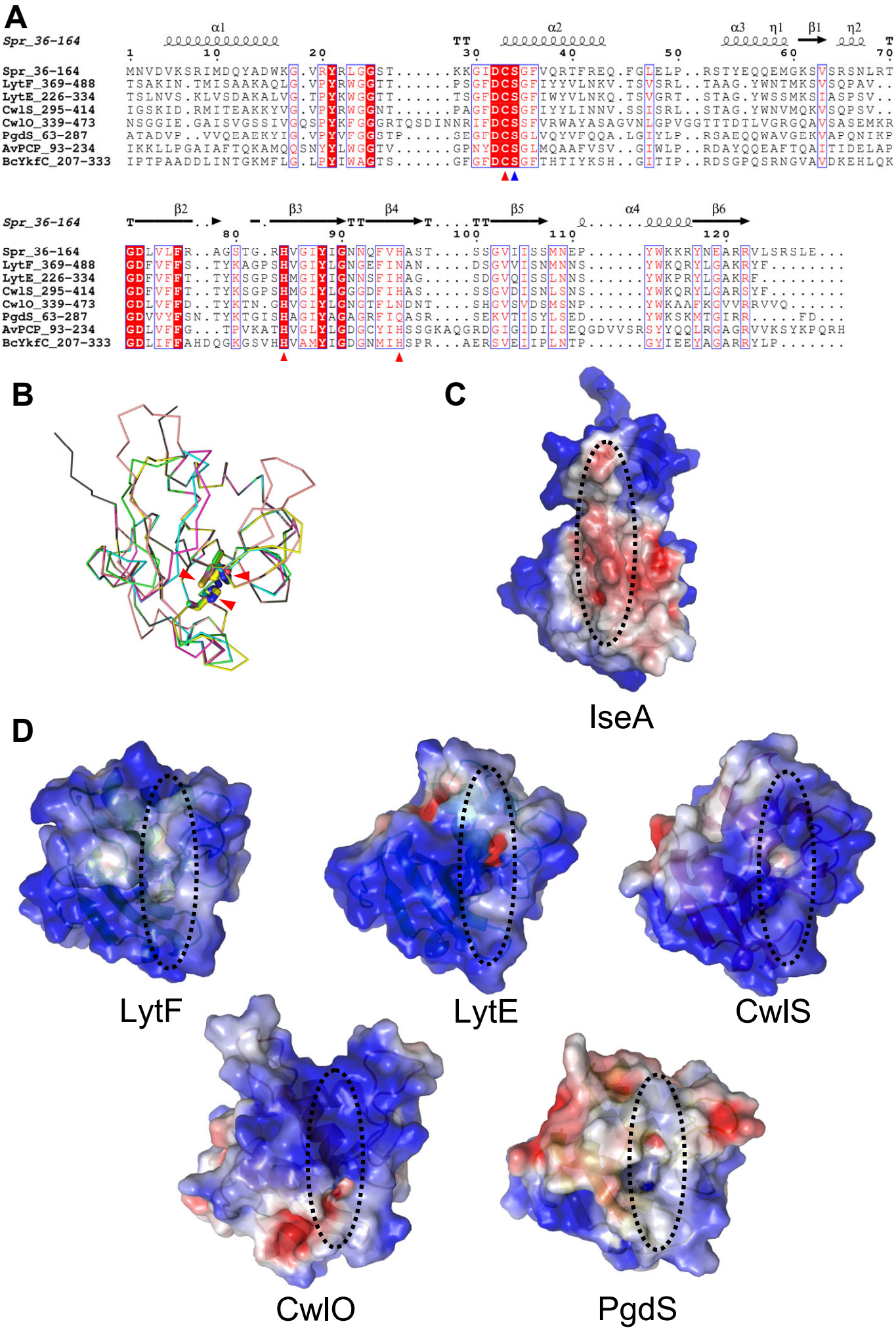

Fig. 9, R. Arai et al., NMR Structure of IseA

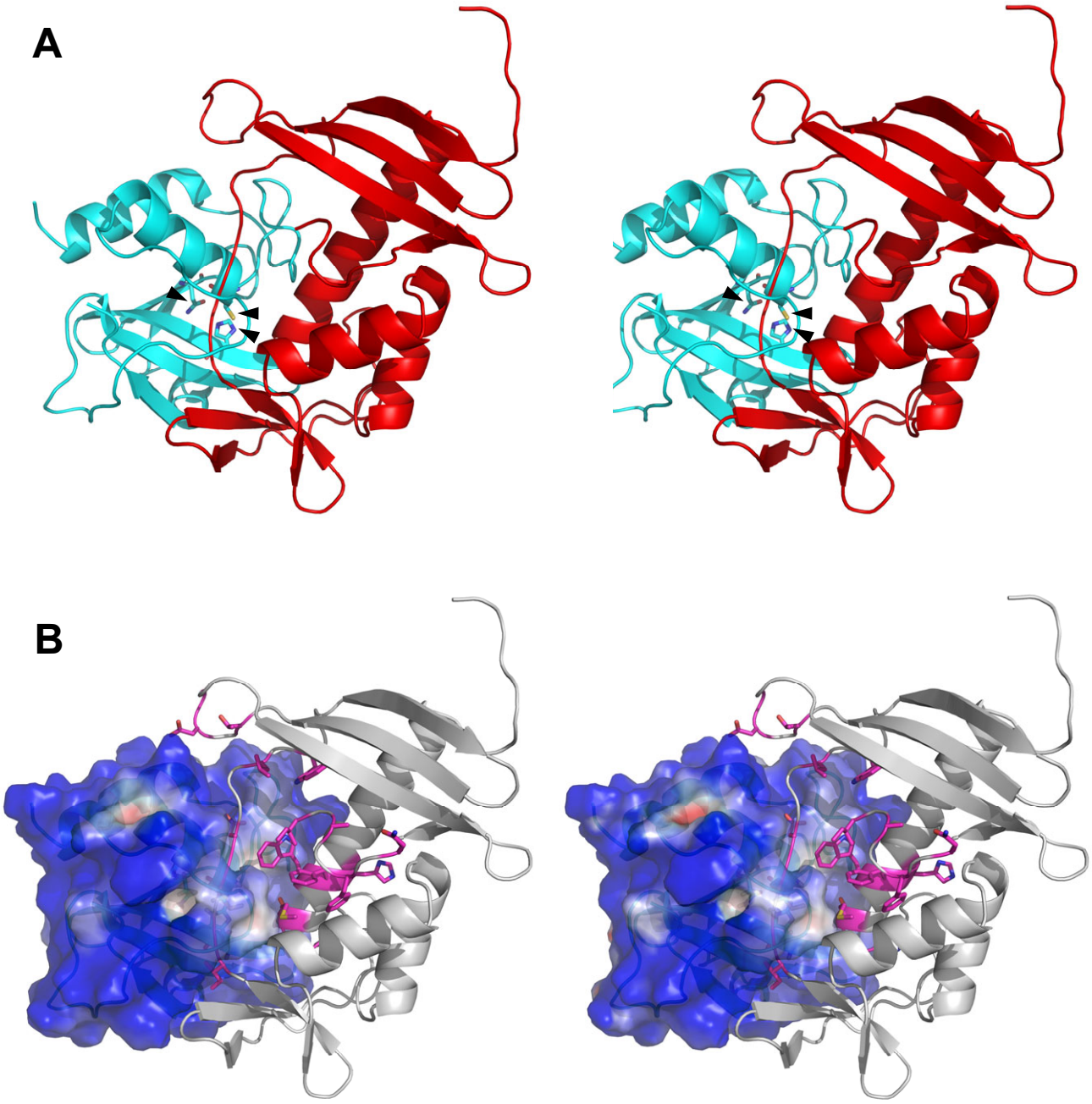

Fig. 10, R. Arai et al., NMR Structure of IseA

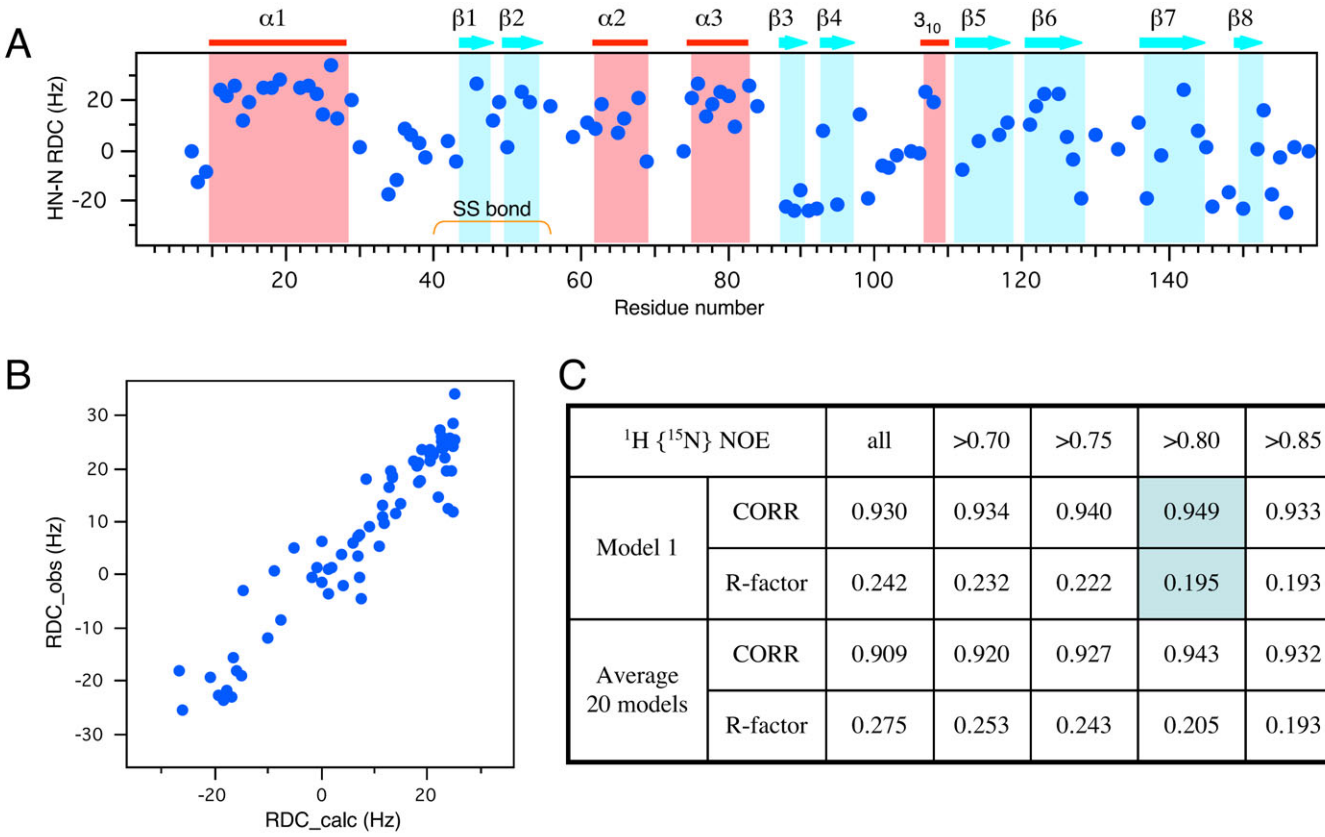

C

^{1}H {^{15}N} NOE		all	>0.70	>0.75	>0.80	>0.85
Model 1	CORR	0.930	0.934	0.940	0.949	0.933
	R-factor	0.242	0.232	0.222	0.195	0.193
Average 20 models	CORR	0.909	0.920	0.927	0.943	0.932
	R-factor	0.275	0.253	0.243	0.205	0.193

Figure S1. Residual dipolar coupling (RDC) analysis of IseA with polyacrylamide gel.
(A) RDC values of ^{1}HN-^{15}N.
(B) A correlation plot between RDC values observed and calculated from Model 1 of the IseA structure. It indicates a high correlation between those (r = 0.949).
(C) A result matrix of correlation analysis between RDC values observed and calculated in Model 1 and average of 20 models of the IseA structure. These analyses support high accuracy of the IseA structure determined by NMR.